

1  
2 Phospholipid localization implies microglial morphology and  
3 function via Cdc42 *in vitro*  
4

5 Kyohei Tokizane<sup>1</sup>, Hiroyuki Konishi<sup>1</sup>, Kumiko Makide<sup>3</sup>, Hiroki Kawana<sup>3</sup>, Shinichi  
6 Nakamuta<sup>2</sup>, Kozo Kaibuchi<sup>2</sup>, Tomohiko Ohwada<sup>4</sup>, Junken Aoki<sup>3</sup>, Hiroshi  
7 Kiyama<sup>1\*</sup>

8  
9 <sup>1</sup>Department of Functional Anatomy and Neuroscience,

10 <sup>2</sup>Department of Cell Pharmacology,

11 Nagoya University, Graduate School of Medicine, Nagoya, 65 Tsurumai-cho,  
12 Showa-ku, Aichi 466-8550, Japan

13 <sup>3</sup>Molecular and Cellular Biochemistry, Graduate School of Pharmaceutical  
14 Sciences, Tohoku University, 6-3, Aoba, Aramaki, Aoba-ku, Sendai, Miyagi  
15 980-8578, Japan

16 <sup>4</sup>Laboratory of Organic and Medicinal Chemistry, Graduate School of  
17 Pharmaceutical Sciences, The University of Tokyo, 7-3-1 Hongo, Bunkyo-ku,  
18 Tokyo 113-0033, Japan

19 Mailing address:

20 Kyohei Tokizane: [tokizane@med.nagoya-u.ac.jp](mailto:tokizane@med.nagoya-u.ac.jp)

21 Hiroyuki Konishi: [konishi@med.nagoya-u.ac.jp](mailto:konishi@med.nagoya-u.ac.jp)

22 Kumiko Makide: [makide@mail.pharm.tohoku.ac.jp](mailto:makide@mail.pharm.tohoku.ac.jp)

23 Hiroki Kawana: [hiroki.kawana.t4@dc.tohoku.ac.jp](mailto:hiroki.kawana.t4@dc.tohoku.ac.jp)

24 Shinichi Nakamuta: [nakamuta@med.nagoya-u.ac.jp](mailto:nakamuta@med.nagoya-u.ac.jp)

25 Kozo Kaibuchi: [kaibuchi@med.nagoya-u.ac.jp](mailto:kaibuchi@med.nagoya-u.ac.jp)

26 Tomohiko Ohwada: [ohwada@mol.f.u-tokyo.ac.jp](mailto:ohwada@mol.f.u-tokyo.ac.jp)

27 Junken Aoki: [jaoki@m.tohoku.ac.jp](mailto:jaoki@m.tohoku.ac.jp)

28 Hiroshi Kiyama: [kiyama@med.nagoya-u.ac.jp](mailto:kiyama@med.nagoya-u.ac.jp)

29 Running Title: Cdc42 localization implies microglia form

30  
31  
32  
33 Abstract: 162 words

34 Introduction: 423 words

35 Material and Methods: 2,556 words

1 Results: 1,827 words  
2 Discussion: 1,502 words  
3 Acknowledgments: 101 words  
4 Author contributions: 82 words  
5 References: 1,384 words  
6 Figure legends: 1,217 words  
7 Number of figures: 7  
8 Movie: 1  
9 Total word count: 9,254 words

10

11 \*Corresponding author: Dr. Hiroshi Kiyama, Department of Functional Anatomy  
12 and Neuroscience, Nagoya University Graduate School of Medicine, 65  
13 Tsurumaicho, Showa-ku, Nagoya, Aichi 466-8550, Japan.  
14 Tel: +81-52-744-2015; Fax: +81-52-744-2027;  
15 E-mail address: [kiyama@med.nagoya-u.ac.jp](mailto:kiyama@med.nagoya-u.ac.jp)

16

#### 17 **Main Points**

- 18 • LysoPS rapidly induces microglia ramification in a receptor independent
- 19 manner.
- 20 • The incorporated LysoPS into microglia is converted to PS and activates
- 21 Cdc42-signalling.
- 22 • LysoPS treatment suppresses the pro-inflammatory microglial phenotype.

23

24 **Key Words:** ramified microglia, lysophospholipid, phosphatidylserine

25

1 **Abstract**

2 Under a quiescent state, microglia exhibit a ramified shape, rather than the  
3 amoeboid-like morphology following injury or inflammation. The manipulation of  
4 microglial morphology *in vitro* has not been very successful, which has impeded  
5 the progress of microglial studies. We demonstrate that lysophosphatidylserine  
6 (LysoPS), a kind of lysophospholipids, rapidly and substantially alters the  
7 morphology of primary cultured microglia to an *in vivo*-like ramified shape in a  
8 receptor independent manner. This mechanism is mediated by Cdc42 activity.  
9 LysoPS is incorporated into the plasma membrane and converted to  
10 phosphatidylserine (PS) *via* the Lands cycle. The accumulated PS on the  
11 membrane recruits Cdc42. Both Cdc42 and PS co-localize predominantly in  
12 primary and secondary processes, but not in peripheral branches or tips of  
13 microglia. Along with the morphological changes LysoPS suppresses  
14 inflammatory cytokine production and NF- $\kappa$ B activity. The present study provides  
15 a tool to manipulate a microglial phenotype from an amoeboid to a fully ramified  
16 *in vitro*, which certainly contributes to studies exploring microglial physiology and  
17 pathology.  
18

## 1 **Introduction**

2 Resident microglia are assumed to be a specialized population of immune cells  
3 in the brain, acting as the first defence in the central nervous system (CNS)  
4 (Kreutzberg 1996). Microglia, under a quiescent state, exhibit a ramified shape  
5 and are continuously surveying nearby brain conditions (Nimmerjahn et al. 2005;  
6 Wake et al. 2009), whereas, in response to injury or inflammatory stimuli, the  
7 microglia dynamically alter their morphology: rapid process protrusion, retraction,  
8 and thickening, as well as cellular migration (Hanisch and Kettenmann 2007).  
9 Activated microglia are capable of returning to a ramified morphology in  
10 conjunction with tissue recovery or a reduction in the inflammatory response  
11 (Ladeby et al. 2005). Although a greater correlation between microglial  
12 morphology and function is assumed, the molecular correlation between  
13 morphology and function remains largely unknown. This is partly due to the lack  
14 of manipulation techniques of microglial morphology *in vitro*. One of the greatest  
15 difficulties in microglial research is the gap between *in vitro* and *in vivo*  
16 morphology and function (Butovsky et al. 2014; Rosenstiel et al. 2001). Primary  
17 cultured microglia routinely exhibit a flat and/or spindle shaped morphology that  
18 is distinct from the typical ramified morphology observed in the steady-state  
19 brain. Manipulation of microglial morphology *in vitro* would be an important  
20 advancement for addressing the mechanisms underlying microglial dynamic  
21 changes of morphology and function.

22 To determine cell polarity, cytokinesis, and morphogenesis, the membrane  
23 characteristics implied by phospholipid localization, asymmetry, and composition  
24 on the plasma membrane are crucial (Das et al. 2012; Yeung et al. 2008). In  
25 yeast, for instance, phosphatidylserine (PS) levels peak during bud emergence,  
26 and cells lacking the phosphatidylserine-synthase gene grow more slowly than  
27 wild-type (WT), implying that phosphatidylserine localization is important for  
28 optimal growth (Fairn et al. 2011). To manipulate phospholipid localization in the  
29 plasma membrane, the application of a lyso-form of phospholipids could be an  
30 alternative tool, although lysophospholipids (LPLs) serve a wide variety of  
31 functions as lipid mediators that are exerted through G protein-coupled  
32 receptors specific to each lysophospholipid (Makide et al. 2014). Because  
33 lysophosphatidylserine (LysoPS), for instance, appears to be incorporated into

1 the cytoplasm, subsequent acylation results in increased PS in the intracellular  
2 membrane domain (Fairn et al. 2011).

3 In this study, we demonstrate that one of the lysophospholipid members,  
4 LysoPS, rapidly and substantially alters the morphology of primary cultured  
5 microglia into a ramified shape. The morphological changes take place in a  
6 receptor independent manner, but are mediated by Cdc42 Rho GTPase activity.  
7 We further reveal that in parallel with the morphological changes LysoPS  
8 suppresses lipopolysaccharide (LPS)-induced inflammatory cytokine production  
9 and NF- $\kappa$ B activity.

10

## 11 ***Materials and Methods***

### 12 *Materials*

13 18:1-LysoPS, 18:0-LysoPS, 18:1-PS, di12:0-PS, 17:0-, 18:1-lysophosphatidyl  
14 acid (LPA), 18:0-lysophosphatidylethanolamine (LPE),  
15 18:0-lysophosphatidylcholine (LPC), liver (90% 18:0-) lysophosphatidylinositol  
16 (LPI) and 18:1-lysophosphatidylglycerol (LPG) were purchased from Avanti  
17 Polar Lipids (Alabaster, AL, USA). 18:1-sphingosine-1-phosphate (S1P) was  
18 from Cayman Chemical (Ann Arbor, MI, USA). LysoPS with various fatty acids  
19 [capric (10:0), lauric (12:0), myristic (14:0), palmitic (16:0) and palmitoleic (16:1)]  
20 and LysoPS analogues with oleic acid (18:1) including deoxy-LysoPS were  
21 synthesized as previously described (Iwashita et al. 2009; Uwamizu et al. 2015).  
22 Eicosatetraenoic (20:4) and docosahexaenoic (22:6) were provided by Ono  
23 Pharmaceutical Co., Ltd (Osaka, Japan). High-selectivity agonist for GPR34  
24 (compound No. 12) (Jung et al. 2016), P2Y10 (compound No. 25) (Jung et al.  
25 2016), and GPR174 (LysoPalloT-C3-ph-m-O-C7) (Ikubo et al. 2015) were  
26 synthesized as previously described. To prepare liposomes, lipids were  
27 dissolved in chloroform in a clean siliconized glass tube, dried under a gentle  
28 stream of nitrogen gas, and further dried under a vacuum for 30 min. The dried  
29 lipid was hydrated, resuspended in phosphate-buffered saline (PBS) containing  
30 0.1% (w/v) fatty acid-free bovine serum albumin (BSA) (Sigma-Aldrich, St Louis,  
31 MO, USA) to a concentration of 2 mM, and sonicated to produce the final  
32 solution in accordance with a previous report (Ikubo et al. 2015). We aliquoted

1 the solutions to avoid freeze-and-thaw cycles and stocked them at  $-80^{\circ}\text{C}$ . The  
2 purity was at least  $> 95\%$ . For inhibitors of signalling molecules, a selective  
3 inhibitor of geranylgeranylation (GGTI 298: #16176) was purchased from  
4 Cayman Chemical. Inhibitors for PKA (KT5720: #420320), PI3K (LY294002:  
5 #440202) and MEK (U0126: #662005) were purchased from Calbiochem (La  
6 Jolla, CA, USA). Inhibitors for ROCK (Y27632: #257-00511) and Rac1  
7 (NSC23766: #180-02491) were purchased from Wako (Osaka, Japan). Inhibitor  
8 for Cdc42 (ML-141: #SML0407) was purchased from Sigma-Aldrich.

### 9 10 *Animals*

11 All efforts were made to minimize animal suffering, and to reduce the number of  
12 animals used. To generate GPR34 KO mice, the GPR34 locus was targeted  
13 using a standard homologous recombination approach in 129-background  
14 embryonic stem cells. Briefly, the GPR34 gene was disrupted with a targeting  
15 vector, which was designed to replace the GPR34 open reading frame in-frame  
16 with a LacZ-neo cassette. GPR34 KO mice were backcrossed to the C57BL/6  
17 background for 12 generations. C57BL/6 WT (SLC, Hamamatsu, Japan) and  
18 GPR34 KO mice were housed with food and water available *ad libitum* in a  
19 temperature ( $23 \pm 1^{\circ}\text{C}$ )- and humidity (50%)-controlled environment on a  
20 12/12-h light/dark cycle (lights on at 09.00 h). All mice were maintained in  
21 accordance with the Guide for the Care and Use of Laboratory Animals (National  
22 Institutes of Health, 1996). The protocol for the animal experiment was approved  
23 by the Animal Ethics Committee of Nagoya University (approval number: 26181,  
24 27204 and 28303).

### 25 26 *Primary cultures*

27 Microglia were obtained from a primary mix-culture in accordance with a  
28 previous report (Konishi et al. 2006). Briefly, brains were collected from WT and  
29 GPR34 KO mice at postnatal day 1 or 2. After removal of the meninges, the  
30 tissue was minced with a razor blade and treated with trypsin (Invitrogen,  
31 Carlsbad, CA, USA) and DNase I (Roche Applied Science, Indianapolis, IN,  
32 USA), and dispersed cells were seeded in a culture flask. After 10–12 d in  
33 culture, detached microglia were collected and plated on 24- or 96-well culture

1 dishes. Microglial cells were plated on non-coated glass coverslips for  
2 immunostaining and scanning electron microscopy (SEM). The purity was >  
3 98%. After 10–12 h, the cultured microglial cells were serum-starved for 4 h, and  
4 then stimulated with 10  $\mu$ M of LysoPS. For quantitative real-time RT-PCR and  
5 NF- $\kappa$ B translocation analysis, microglial cells were stimulated with 100 ng/ml of  
6 LPS (#L4516; Sigma-Aldrich) for 12 h prior to serum starvation. Cortical neurons  
7 were prepared from cerebra of embryonic day (E) 16 embryonic C57BL/6 mice.  
8 Neurons were seeded on PLL-coated 12-mm round glass coverslips placed on  
9 the bottom of 24-well culture dishes ( $1.5 \times 10^5$  cells/well) and precultured in  
10 Neurobasal medium (Invitrogen) containing 0.05 mg/ml penicillin/ streptomycin  
11 (Invitrogen), 0.5 mM glutamine, and B27 supplement (Invitrogen) for 4 d. Cortical  
12 astrocytes were isolated and cultured from postnatal day 1 to 3 pups from  
13 C57BL/6 mice as described (Schildge et al. 2013) and were maintained at 37°C  
14 in a CO<sub>2</sub> incubator. The cultured neurons and astrocytes were serum-starved for  
15 4 h, and then stimulated with 10  $\mu$ M of LysoPS.

16

### 17 *SEM*

18 Microglial cells were collected 60 min after LysoPS application and fixed in 0.1 M  
19 phosphate buffer (PB) containing 2.5% glutaraldehyde overnight at 4°C. Cells  
20 were post-fixed in 1% OsO<sub>4</sub> in 0.1 M PB for 30 min at room temperature (RT),  
21 and dehydrated in an ethanol gradient at RT. After dehydration in absolute  
22 ethanol three times, samples were incubated in t-butyl alcohol for 30 min at 30°C  
23 three times, and then kept in t-butyl alcohol overnight at 4°C. Specimens were  
24 dried using a freeze dryer (VFD-21S; Vacuum Device, Ibaraki, Japan), coated  
25 with osmium by ion sputter (HPC-30W; Vacuum Device), and observed with a  
26 scanning electron microscope (JSM-7610; JEOL, Tokyo, Japan).

27

### 28 *Time-lapse imaging of cultured cells*

29 For time-lapse imaging, microglial cells were directly plated onto a glass base  
30 dish (#3971-035; Iwaki, Tokyo, Japan). Images were collected at 2 min intervals  
31 using an imaging microscope system (LCV110; Olympus, Tokyo, Japan). Cells  
32 were maintained at 37°C in 5% CO<sub>2</sub> throughout the experiment. The time-lapse  
33 images were used for quantitative analysis of morphologies, as well as dynamics

1 of microglial processes and migration velocity. The speed of microglial migration  
2 was determined by tracking microglial cell bodies using MetaMorph 7.5.6.0  
3 software (Universal Imaging, Media, PA, USA).

#### 4 *Immunocytochemistry and image analysis*

6 Microglial cells cultured on glass coverslips were fixed in 0.1 M PBS, pH 7.4,  
7 containing 4% paraformaldehyde (PFA) for 10 min at RT. Then immunostaining  
8 was done according to a previous method (Konishi et al. 2010) using rabbit  
9 anti-beta III tubulin (1:2000, RRID: AB\_444319; Abcam, Cambridge, UK), mouse  
10 anti-GFAP (1:1000, RRID: AB\_477010; Sigma-Aldrich), rabbit anti-Iba1 (1:1,000,  
11 RRID: AB\_839504; Wako) and rabbit anti-p65 (1:100, RRID: AB\_632037; Santa  
12 Cruz Biotech, Santa Cruz, California, USA) as primary antibodies and Alexa  
13 Fluor 488 or 594-labelled anti-rabbit IgG (1:1,000; Invitrogen) as a secondary  
14 antibody. Actin was visualized by Alexa Fluor 594-labelled phalloidin (1:100;  
15 #A12381; Invitrogen). Nuclei were stained with DAPI solution (1:5000;  
16 #340-07971; Dojindo Laboratories, Kumamoto, Japan). Images were acquired  
17 using fluorescent microscopy (BZ-9000; Keyence, Osaka, Japan). The line-scan  
18 intensity distribution analysis was performed using the Image J software (NIH,  
19 Bethesda, MD, USA).

#### 21 *Determination of cell shape and form factor*

22 To quantitatively assess the shape of microglia, we employed the form factor.  
23 Cell circumferences were drawn using the freehand selections tool, and the area  
24 and perimeter of each cell was determined using Image J. Then the form factor  
25 was calculated using the formula  $(4\pi \times \text{area}/[\text{perimeter}]^2)$  as previously  
26 described (Wilms et al. 1997). Form factor indicates complexity of cell shape: 1 =  
27 an exactly round cell; value closer to 0 = highly bushy cell. A total of 20 cells  
28 were randomly selected from at least three independent experiments and were  
29 analyzed.

#### 31 *LC-MS/MS analysis*

32 18:1-LysoPS, 17:0-LPA, and di12:0-PS were dissolved in methanol using a  
33 water bath sonicator, and stored at  $-20^{\circ}\text{C}$ . Microglia cells ( $1 \times 10^5$ ) were

1 collected in a test tube with 200  $\mu$ l of methanol and crushed using a water bath  
2 sonicator. After centrifugation at 21,500  $\times$  g, the supernatant was added to  
3 di12:0-PS (10  $\mu$ M, final concentration) or 17:0-LPA (100 nM, final concentration).  
4 After being passed through a filter (0.2  $\mu$ m pore size, YMC, Kyoto, Japan), the  
5 samples (10  $\mu$ l for PS analysis or 20  $\mu$ l for LysoPS analysis) were subjected to  
6 LC-MS/MS as previously described with some modifications (Inoue et al. 2011).  
7 For LysoPS, LC separation was performed using the UltiMate 3000 HPLC  
8 (Thermo Fisher Scientific, Waltham, MA, USA) with C18 CAPCELL PAK ACR  
9 columns (100 mm  $\times$  1.5 mm, Shiseido, Tokyo, Japan) using a linear gradient of  
10 solvent A (5 mM ammonium formate in water) and solvent B (5 mM ammonium  
11 formate in 95% (v/v) acetonitrile). MS/MS was carried out on a TSQ Quantiva  
12 Triple-Stage Quadrupole mass spectrometer (Thermo Fisher Scientific). LysoPS  
13 were monitored in the multiple reaction-monitoring (MRM) mode with neutral  
14 loss of the 87 Da fragment of [M-H]<sup>-</sup> ions. PS analysis was performed similar to  
15 the LysoPS analysis, except that the HPLC system consisted of a NANOSPACE  
16 SI-II (Shiseido) and C8 CAPCELL PAK UG120 column (150 mm  $\times$  1.5 mm,  
17 Shiseido), and a TSQ Quantum Ultra triple quadrupole mass spectrometer  
18 (Thermo Fisher Scientific) were used. PS analyses were performed in the MRM  
19 mode with neutral loss of 185 Da fragment of [M+H]<sup>+</sup> ions.

20

### 21 *Protein purification*

22 The plasmids of pGEX-evectin2- pleckstrin homology (PH) domain (Uchida et al.  
23 2011) and the pGEX-Pak1-PBD domain were transformed into *Escherichia coli*  
24 BL21 (DE3), and protein expressions were induced by addition of 1 mM  
25 isopropyl- $\beta$ -D-thiogalactopyranoside to exponential-phase bacteria. After 4 h at  
26 37°C, the bacteria were harvested and lysed with PBS containing 1% Triton  
27 X-100 and protease inhibitor cocktail (Complete EDTA-free; Roche) for 30 min at  
28 4°C. The supernatants were subsequently incubated with  
29 glutathione-Sepharose 4B (GE Healthcare Life Sciences, Buckinghamshire, UK)  
30 for 1 h at 4°C, and the bound proteins were eluted by adding 10 mM reduced  
31 glutathione in 50 mM Tris-HCl, pH 8.0. After removal of glutathione by dialysis  
32 against PBS, the proteins were checked by SDS-PAGE, followed by Coomassie  
33 Brilliant Blue R-250 staining, and stored at -80°C until further use.

1  
2 *Immunolabelling of PS by evectin-2 PH domain-glutathione S-transferase (GST)*  
3 *probe*

4 The cultured microglia were fixed in PBS, pH 7.4, containing 4% PFA for 10 min  
5 at RT. They were then washed in PBS, pH 6.0, at least three times for 30 min,  
6 and incubated with the evectin-2 PH domain with glutathione S-transferase  
7 (GST-evt-2-PH probe) in PBS, pH 6.0, (3 µg/ml) for 30 min at RT. After washing  
8 in PBS at least three times for 30 min, the cells were blocked with 1% BSA, 0.3%  
9 Triton-X in PBS for 1 h, incubated with rabbit anti-GST (1:1000, RRID:  
10 AB\_67419; Bethyl Laboratories, Montgomery, TX, USA) and/or mouse  
11 anti-Cdc42 (1:200, RRID: AB\_627233; Santa Cruz) primary antibody overnight,  
12 and washed in PBS at least three times for 30 min. Signals were detected with  
13 Alexa 488- or 647-labelled donkey anti-rabbit or anti-mouse IgG (1:1000 dilution;  
14 Invitrogen). We have examined the use of another antibody recognizing a  
15 different epitope of Cdc42 (anti-rabbit Cdc42, 1:100, RRID: AB\_631213; Santa  
16 Cruz) and obtained the same staining as monoclonal mouse antibody.  
17 Additionally, we confirmed the specificity of monoclonal mouse antibody by  
18 using an anti-mouse CD16/CD32 antibody (1:100, RRID: AB\_467132;  
19 eBioscience, San Diego, CA, USA) as a blocking system of the FC receptor. We  
20 did not find any non-specific antibody binding with the FC receptor. Actin was  
21 visualized by Alexa Fluor 594-labelled phalloidin. The point mutant K20E of  
22 GST-evt-2-PH probe, in which Lys20 was changed to Glu and lacked the ability  
23 to bind to the PS head group (Uchida et al. 2011), did not show immune-positive  
24 signals in this method.

25  
26 *Adeno-associated virus (AAV) preparation and infection*

27 Rac1 and Cdc42 cDNA were inserted into the pAAV-CAG-EGFP-MCS-WPRE  
28 vector of the AAV Helper-Free System (Stratagene, La Jolla, CA, USA), and  
29 purified according to previous methods (Inutsuka et al. 2014; Lazarus et al.  
30 2011). Briefly, HEK293T cells (Cell BioLabs, Inc., San Diego, CA, USA) were  
31 transfected with the above-described pAAV vector, pHelper (Cell BioLabs Inc.),  
32 and pAAV-DJ (Cell BioLabs Inc.) using a standard calcium phosphate method.  
33 After 3 d, the transfected cells were collected, re-suspended in PBS, and lysed

1 by four cycles of freeze-thawing. The cell extract was treated with Benzonase  
2 nuclease (Merck, Darmstadt, Germany) at 45°C for 15 min and centrifuged twice  
3 at 15,000 × g for 10 min, and the supernatant was collected. The virus titre in the  
4 supernatant was determined by quantitative PCR (#6233: Takara, Tokyo,  
5 Japan), and used for infection. Plated pure microglia were incubated with  
6 virus-containing medium at  $1.6 \times 10^4$  copies/cell for 1 h, and then the medium  
7 was replaced with normal culture medium without AAV. Microglial cells at 6 d  
8 after infection were used for immunocytochemical analysis.

### 9 10 *Rho GTPase activation assays*

11 To determine Rac1 and Cdc42 activation, we performed a GST-pulldown assay  
12 using the Rac1 and Cdc42-interactive binding domain of Pak1. Microglial cells  
13 were serum-starved for 4 h, and then stimulated with 10 μM LysoPS. Microglia  
14 cells were harvested with cold lysis buffer containing 50 mM Tris-HCl, pH 7.5,  
15 500 mM NaCl, 0.5% Nonidet-P40, 1 mM EGTA, 10 mM MgCl<sub>2</sub>, 0.1 mM APMSF,  
16 2.5 μg/ml of aprotinin, 2.5 μg/ml of leupeptin and 20 μg of Pak1-PBD GST-fusion  
17 protein. The lysates were centrifuged at 15,000 × g for 2 min, and the  
18 supernatant was incubated with glutathione-Sepharose 4B (#17-0756-01; GE  
19 Healthcare Life Sciences) for 30 min at 4°C. Sepharose was washed with PBS,  
20 and the bound proteins were eluted by addition of 18 μl of sample buffer. A total  
21 of 15 μl of eluate and total cell lysates were loaded onto SDS-PAGE. After  
22 semidry blotting, PVDF membranes (Millipore, Billerica, MA, USA) were blocked  
23 with 5% skim milk (Wako) in Tris-buffered saline with 0.1% Tween 20 (TBS-T)  
24 and incubated with primary antibodies diluted in blocking solution for 10–12 h at  
25 4°C. Primary antibodies were as follows: rabbit anti-Rac1 (1:200, RRID:  
26 AB\_2238100; Santa Cruz), mouse anti-Cdc42. Horseradish  
27 peroxidase-conjugated secondary antibodies (GE Healthcare Life Sciences) and  
28 ECL (GE Healthcare Life Sciences) were used for detection. If necessary,  
29 membranes were stripped with stripping buffer (100 mM β-mercaptoethanol, 2%  
30 SDS, 62.5 mM Tris, pH 6.8) for 20 min at 55°C.

### 31 32 *Quantitative real-time RT-PCR*

1 Quantitative real-time RT-PCR (qPCR) was performed as previously described  
2 (Tokizane et al. 2013). For primary microglial cells, SYBR Green Cells-to-Ct Kit  
3 (Thermo Fisher Scientific) was used to obtain total RNA and synthesize cDNA in  
4 accordance with manufacturer instructions. qPCR was performed using SYBR  
5 Green (Thermo Fisher Scientific) with the StepOnePlus Real-Time RT-PCR  
6 System (Thermo Fisher Scientific). The following primers were used: GPR34  
7 forward: 5'-ATATGCTACAACAGCCCGGA-3'; GPR34 reverse:  
8 5'-GAACCGAAAGGCATGGTAAG-3'; P2Y10 forward:  
9 5'-TAGGTACGATGTGGGCATCA-3'; P2Y10 reverse:  
10 5'-CAGCAAAGCGAGAATCTGTG-3'; GPR174 forward:  
11 5'-CCATTTGGTCCTGGTCTCTG-3'; GPR174 reverse:  
12 5'-CTTCGCACACTGATGCAGAC-3'; IL1- $\beta$  forward:  
13 5'-ACAGAATATCAACCAACAAGTGATATTCTC-3'; IL1- $\beta$  reverse:  
14 5'-GATTCTTTCCTTTGAGGCCCA-3'; IL6 forward:  
15 5'-ATCCAGTTGCCTTCTTGGGACTGA-3'; IL6 reverse:  
16 5'-TAAGCCTCCGACTTGTGAAGTGGT-3'; TNF- $\alpha$  forward:  
17 5'-AGCCGATGGGTTGTACCTTGTCTA-3'; TNF- $\alpha$  reverse:  
18 5'-TGAGATAGCAAATCGGCTGACGGT-3'; iNOS forward:  
19 5'-GGCAGCCTGTGAGACCTTTG-3'; iNOS reverse:  
20 5'-GAAGCGTTTCGGGATCTGAA-3'; IL10 forward:  
21 5'-GGTTGCCAAGCCTTATCGGA-3'; IL10 reverse:  
22 5'-ACCTGCTCCACTGCCTTGCT-3'; TGF- $\beta$  forward:  
23 5'-CCGCAACAACGCCATCTATG-3'; TGF- $\beta$  reverse:  
24 5'-TGCCGTACAACCTCCAGTGAC-3'; IGF-1 forward:  
25 5'-GCTGGTGGATGCTCTTCAGT-3'; IGF-1 reverse:  
26 5'-TAGGGACGGGACTTCTGAG-3'; GAPDH forward:  
27 5'-CAAGGTCATCCCAGAGCTGA-3'; GAPDH reverse:  
28 5'-CGGCACGTCAGATCCACGAC-3'. qPCR reaction conditions were as  
29 follows: 1 cycle of 95°C for 20 s, 40 cycles of 95°C for 3 s, and 60°C for 30 s. At  
30 the end of the PCR, the samples were subjected to a melting analysis to confirm  
31 amplicon specificity. Relative gene expression ( $\Delta$ Ct value) was calculated based  
32 on the Threshold Cycle (Ct) of the reference gene (GAPDH) and target gene

1 ( $\Delta Ct = Ct_{\text{target gene}} - Ct_{\text{reference gene}}$ ).  $\Delta\Delta Ct$  was calculated as  $\Delta Ct_{\text{LPS treatment}} - \Delta Ct_{\text{LPS +}}$   
2 LysoPS treatment, and  $2^{-\Delta\Delta Ct}$  was determined as the fold change.

### 3 4 *Statistical analysis*

5 No statistical methods were used to predetermine sample sizes, but the sample  
6 sizes used are similar to those generally employed in the field. No data points  
7 were removed from statistical analysis. All data were analyzed using the  
8 GraphPad Prism 7 software program. The statistical analyses were performed  
9 using a one-way analysis of variance (ANOVA) followed by or Dunnett's *post*  
10 *hoc* test, a paired *t*-test. For single comparisons between two groups, an  
11 unpaired Student's *t*-test was applied. Mann-Whitney U-tests were applied when  
12 data were not normally distributed or there was no equal variance. Data were  
13 presented as mean  $\pm$  S.D. or  $\pm$  S.E.M., and differences were considered to be  
14 significant for values at  $P < 0.05$ .

## 15 16 **Results**

### 17 ***LysoPS rapidly induces microglia ramification***

18 We first examined the effect of 18:1-LysoPS on primary cultured microglia in  
19 serum-free conditions. A higher dose of LysoPS (10  $\mu\text{M}$ ) resulted in rapid and  
20 significant changes in microglial morphology, whereas both 0.1  $\mu\text{M}$  and 1  $\mu\text{M}$  did  
21 not alter morphology. To observe precise microglial morphology, we employed  
22 SEM. Under normal culture conditions, the microglial cells exhibited an  
23 amoeboid-like shape with no clear fine processes (Fig. 1A) or a spindle-like  
24 shape. Conversely, LysoPS-treated microglia exhibited the typical ramified  
25 morphology with a smaller cell body and several long processes whose tips were  
26 growth cone-like shape (Fig. 1B). More than 90% of microglia synchronously  
27 showed similar changes. In contrast, primary neurons and primary astrocytes did  
28 not show any difference in morphological analysis between vehicle and LysoPS  
29 treatment (Fig. 1C, D). Time-lapse imaging demonstrated that LysoPS induced  
30 morphological changes over a relatively short time period (Fig. 1E and Movie 1).  
31 The microglia extended their processes and increased the number of processes  
32 during the first 20 min following LysoPS treatment, and the number and length of  
33 processes were maintained for more than 2 h (Fig. 1E, F). Intriguingly, the tips of

1 the extended processes kept moving, protruding and retracting in a manner  
2 similar to the quiescent state of microglia *in vivo* (Fig. 1G). Next, the microglial  
3 migration trajectories were re-plotted by aligning the starting point of each  
4 trajectory at the same origin and measuring the velocity of microglial movement.  
5 LysoPS treatment dramatically reduced motility and velocity (Fig. 1H, I). These  
6 data indicate that LysoPS induced the ramification of cultured microglia and  
7 reduced motility of cell bodies, with exception of the tips of processes,  
8 suggesting that this morphology and behaviour closely mimicked ramified  
9 microglia *in vivo*.

### 11 ***Microglial ramification by LysoPS is not mediated through known*** 12 ***receptors***

13 Recently, some orphan G protein-coupled receptors (GPCRs) have been  
14 deorphanized and identified as LysoPS receptors. These include GPR34,  
15 P2Y10, and GPR174, all of which belong to the P2Y family. Therefore, we  
16 examined expression profile of these LysoPS receptors in microglia through  
17 real-time RT-PCR. Among those examined, only GPR34 mRNA was highly  
18 expressed by cultured microglia, and mRNA expression levels of other receptors  
19 were lower, suggesting that GPR34 is the dominant LysoPS receptor in  
20 microglia (Fig. 2A). We further examined the effects of previously identified  
21 receptor agonists (Ikubo et al. 2015; Jung et al. 2016), and found that only  
22 LysoPS is effective (Fig. 2B). For quantification of morphology, we measured the  
23 cell area and perimeter values of individual cells to calculate the form factor  
24 (Wilms et al. 1997). The measurement of the form factor clearly indicated that  
25 only LysoPS was effective in morphological change (Fig. 2C). To further confirm  
26 that morphological change by LysoPS took place in a GPR34 independent  
27 manner, we used GPR34-deficient microglial cells. This experiment clearly  
28 demonstrated the effect of LysoPS was effective even in GPR34-deficient  
29 microglia (Fig. 2D). When LysoPS was applied to GPR34-deficient microglia,  
30 quantification by the form factor indicated a value of  $0.02 \pm 0.002$ , whereas  
31 vehicle-treated GPR34-deficient microglia showed a form factor of  $0.33 \pm 0.025$   
32 (Fig. 2D). Additionally, the Gi and Gs inhibitors [pertussis toxin (PTX) and NF449,  
33 respectively] did not affect the LysoPS-induced changes (data not shown).

1 These results indicate that the previously identified LysoPS receptors were not  
2 involved in microglial ramification induced by LysoPS.

3  
4 ***A specific lysophospholipid group is capable of altering microglial***  
5 ***morphology***

6 Several LysoPS species with various fatty acids are known, although the  
7 endogenous species are restricted *in vivo*. Among various fatty acid lengths,  
8 LysoPS with stearic acid (18:0) or oleic acid (18:1) was the most effective in  
9 altering the microglial form to a ramified shape. The LysoPS species with shorter  
10 or longer fatty acids were less effective (Fig. 3A, B).

11 Under serum-free conditions, we then compared the efficiency of LysoPS with  
12 other LPLs, such as 18:1-LPA, 18:1-S1P, 18:0-LPE, 18:0-LPC, 18:0-LPI,  
13 18:1-LPG and 18:1-PS. Among them, LysoPS was most effective; LPA, S1P,  
14 LPE, and PS did not alter morphologies. Intriguingly, a few lysophospholipids,  
15 such as LPC, LPI, and LPG, induced microglial ramification to some extent (Fig.  
16 3C, D). This suggests the involvement of head polarity; possibly a negative  
17 charge may be important in this function.

18  
19 ***LysoPS is rapidly incorporated into microglial cells and converted to PS***

20 LysoPS is rapidly incorporated into the membrane and flipped to its inner  
21 monolayer in yeast (Fairn et al. 2011). We then examined the incorporation of  
22 exogenous LysoPS into microglia using LC-MS/MS. After 10 min or 1 h of  
23 LysoPS (18:1) treatment, microglial cells were quickly washed and harvested to  
24 measure the lipid profile by LC-MS/MS. Ten minutes after LysoPS treatment,  
25 LysoPS (18:1) in the microglial cells was dramatically increased (more than  
26 190-fold), and the level decreased slightly after 1 h. Simultaneously the  
27 significant increase in PS (38:5; 18:1 and 20:4) was observed, which was >  
28 10-fold after 10 min. Further increase at 1 h (20–40 fold) suggested that PS was  
29 synthesized in microglial cells, likely by membrane-bound acyltransferases (Fig  
30 4A). To further examine whether LysoPS was converted into PS in microglia, we  
31 used LysoPS analogs which did not have the *sn*-2 or *sn*-1 hydroxyl group  
32 (2-deoxy-LysoPS, or 1-deoxy-LysoPS). Both deoxy-LysoPSs failed to induce  
33 microglial ramification (Fig. 4B), suggesting that exogenously applied LysoPS is

1 rapidly incorporated and converted to PS by acyltransferase (Lands cycle). The  
2 increase in intracellular PS was further examined by using a fusion protein of  
3 GST-evt-2-PH, which specifically binds to O-phospho-L-serine, the head group  
4 of PS (Uchida et al. 2011). Immunocytochemistry using anti-GST antibody  
5 clearly revealed an increase in GST-evt-2-PH in LysoPS-treated microglia (Fig.  
6 4C). These results suggest that microglial PS was highly induced by LysoPS  
7 treatment, and the increase was consistent with LC-MS/MS results.

### 8 9 ***LysoPS induces Cdc42-signalling pathways in microglia***

10 A prominent morphological change in cells is often accompanied by specific  
11 intracellular signalling activation. Therefore, we investigated the involvement of  
12 major intracellular signal pathways in morphological change induced by LysoPS.  
13 We examined the effects of various inhibitors on major signalling in  
14 LysoPS-treated microglia. Inhibitors for PKA (KT5720), PI3K (LY294002), ROCK  
15 (Y27632), and MEK (U0126) did not inhibit microglial ramification in  
16 LysoPS-treated conditions. However, the Cdc42 and Rac1 selective inhibitors,  
17 ML141 and NSC23766 respectively, suppressed the effect of LysoPS, although  
18 Rac1 inhibitor had less effect than Cdc42 (Fig. 5A).

19 We then examined the involvement of Cdc42 or Rac1 in microglial ramification  
20 using dominant negative (DN) mutants of Cdc42 and Rac1. Although  
21 transfection efficiency of cultured primary microglia is extremely low, even with  
22 viral vectors, the AAV vector expressing EGFP and either Rac-N17 or  
23 Cdc42-N17 were successfully transfected by a minor number of microglial cells.  
24 Although EGFP and Rac1-N17 expressing microglia did respond to LysoPS, the  
25 EGFP and Cdc42-N17 expressing microglia failed to exhibit the ramification  
26 morphology (Fig. 5B, C), suggesting that Cdc42 could be a key molecule in the  
27 transformation of microglia by LysoPS.

28 We next examined Cdc42 activation by LysoPS application using a pulldown  
29 system to detect the GTP-bound active form of Rac1 and Cdc42. Concomitant  
30 with the DN experiments, LysoPS activated Cdc42 GTPase, but not Rac1 (Fig.  
31 5D, E). These findings suggest that Cdc42 activation was critical for  
32 transformation of microglia by LysoPS.

33

1 ***Cdc42 binding to the PS membrane head group is essential for altering***  
2 ***microglial morphology***

3 To reveal alterations in intracellular localizations of Cdc42 and PS after LysoPS  
4 treatment, cultured microglia were stained with antibodies specific to Cdc42 and  
5 GST-evt-2-PH protein. In the vehicle-treated microglia, evelctin-2 expression was  
6 very weak and found mainly in recycling endosomes (Uchida et al. 2011) and  
7 weakly in the cytoplasmic membrane. LysoPS treatment dramatically increased  
8 evelctin-2 expression in the cytoplasm and thick primary and secondary  
9 processes, but not in further branched peripheral processes and tips.  
10 Expression of Cdc42 after LysoPS appeared similar to evelctin-2 after LysoPS  
11 treatment (Fig. 6A, B). High-power magnification of the primary processes  
12 demonstrated a dotted-shaped expression pattern of evelctin-2 and Cdc42, with  
13 overlap of expression (Fig. 6C).

14 Previous results have demonstrated that Rho GTPases, such as Cdc42,  
15 interact with PS-containing bilayers through the polybasic motif (PBM) *via*  
16 isoprenylation (Finkielstein et al. 2006). Prenylation is an important lipid  
17 modification of proteins, and it plays critical roles in regulating protein-membrane  
18 interactions. Isoprenylation (geranylgeranylation) of Cdc42 is also necessary for  
19 the association with PS (Finkielstein et al. 2006) and subsequent activation  
20 (Henry et al. 2006). To determine whether Cdc42 geranylgeranylation was  
21 implicated in microglial ramification, we employed a selective inhibitor of  
22 geranylgeranylation (GGTI 298), showing that 20  $\mu$ M GGTI 298 treatment  
23 partially suppressed microglial ramification, although localization of both  
24 evelctin-2 and Cdc42 appeared similar (Fig. 6D). However, a higher dose of  
25 GGTI 298 (50  $\mu$ M) completely suppressed the ramification induced by LysoPS,  
26 and localization of evelctin-2 and Cdc42 appeared in distinct intracellular  
27 membrane structures (Fig. 6E), suggesting that the interaction between the PS  
28 head group and Cdc42 by geranylgeranylation was critical for altering microglial  
29 morphology from an amoeboid shape to a ramified shape *in vitro*.

30  
31 ***LysoPS treatment suppress the LPS-induced pro-inflammatory microglial***  
32 ***phenotype***

33 The functional consequence of ramified microglia treated by LysoPS remains

1 intriguing. It was previously thought that there was an empirical correlation  
2 between microglial morphology and function. Therefore, we examined mRNA  
3 expression levels of inflammatory cytokines, such as IL1- $\beta$ , IL6, TNF- $\alpha$  and  
4 iNOS after LysoPS treatment using primary cultured microglia from WT and  
5 GPR34-deficient mice. Prior to LysoPS treatment, LPS was pretreated to induce  
6 an inflammatory phenotype. mRNA expression of all cytokines, except iNOS,  
7 were significantly downregulated by LysoPS treatment compared with vehicle  
8 treatment in WT microglia (Fig. 7A). We also examined mRNA expression of the  
9 anti-inflammatory cytokine IL-10 and the microglia-derived growth factors TGF- $\beta$   
10 and IGF-1. Expression levels of IL-10, TGF- $\beta$ , and IGF-1 mRNA remained  
11 unaltered by LysoPS (Fig. 7A). A similar response pattern was observed in  
12 microglia from GPR34 knockout mice, with exception to IL-10 (Fig. 7B).

13 Other inflammatory associated marker, such as NF- $\kappa$ B, was examined. As  
14 shown in previous studies (Bonizzi and Karin 2004; May and Ghosh 1998; Ni et  
15 al. 2015), the transcription factor NF- $\kappa$ B is an established regulator of expression  
16 of numerous proinflammatory cytokine genes. We examined the subcellular  
17 localization of the NF- $\kappa$ B RelA (p65) subunit after LysoPS treatment. Because  
18 most of the NF- $\kappa$ B p65 subunit was in the microglial cytoplasm following both  
19 vehicle and LysoPS treatments under normal conditions, we stimulated the  
20 nuclear localization of the p65 subunit by LPS, which induced a clear  
21 accumulation of the p65 subunit in microglial nuclei. Under this LPS-activated  
22 condition, LysoPS was applied, which suppressed LPS-induced nuclear  
23 translocation of the p65 subunit (Fig. 7C). Line-scanning analysis clearly  
24 demonstrated the intensity of the intracellular localization of the p65 subunit (Fig.  
25 7D). Under the above-mentioned conditions, the subcellular localization of the  
26 p65 was quantified and presented in Fig. 7E. In vehicle- and LysoPS-treated  
27 cells, > 90% of microglial cells had p65 subunit localization in the cytoplasm.  
28 Conversely, in most LPS-treated cells, the p65 subunit was localized in the  
29 nuclei. LysoPS treatment suppressed nuclear localization of the p65 subunit by  
30 > 50% under the LPS-treated condition. These data indicate that  
31 LysoPS-treatment elicited functional alterations, as well as morphological  
32 changes, in microglia.

33

1 **Discussion**

2 Results from the present study showed that LysoPS induced fully ramified  
3 microglia that accompanied a quiescent function *in vitro*; LysoPS treatment  
4 induced a ramified morphology from an amoeboid or spindle (bipolar) shaped  
5 morphology, and the function changed from pro-inflammatory to quiescent.  
6 Intriguingly, this morphological change was receptor independent, and other  
7 cultured neuronal cells, such as neurons and astrocytes, did not respond to  
8 LysoPS in terms of morphological changes (Fig. 1C, D), suggesting that LysoPS  
9 mediated changes occur specifically in microglia.

10

11 The microglial manipulations including ramification are sought to bring about  
12 therapeutic benefits for patients who suffer from neuropathic pain (Tsuda et al.  
13 2003), neurodegenerative diseases (Boillee et al. 2006), and even mental  
14 disorders (Bayer et al. 1999; Morgan et al. 2010), although some attempts have  
15 been made to induce ramified shapes in microglia *in vitro* (Rosenstiel et al.  
16 2001). To induce a ramified shape in primary cultured microglia, the stromal  
17 cell-derived factor (SDF)-1a, CSF-1 (M-CSF), and a combination of  
18 GM-CSF/IL-34 were previously examined (Muessel et al. 2013), (Neubrand et al.  
19 2014), (Ohgidani et al. 2014). However, these morphological changes require  
20 relatively longer periods: 24 h (SDF-1a), 48 h (CSF-1), and 14 d (GM-CSF/IL-34).  
21 The SDF-1a induced actin-dependent cell spreading through CXCR4 in primary  
22 cultured microglia, and the morphology of microglial processes was short and  
23 relatively flat (Muessel et al. 2013). CSF-1 induced microglial ramification with  
24 numerous short and thick processes, and this required activation of PI3K/Akt,  
25 Cdc42, and Rac1 (Neubrand et al. 2014). Morphology of the above-mentioned  
26 ramified microglia exhibited processes, but precise process morphology was  
27 distinct from those observed *in vivo*. In the *in vivo* quiescent state, microglial  
28 morphology is characterized by a relatively small soma with several thin long  
29 processes, which also have thin branches and the tips of these branches are  
30 ruffled and dynamically moving. More recently, Ohgidani et al. (Ohgidani et al.  
31 2014) succeeded in inducing ramified microglia-like cells from monocytes, which  
32 were more similar to brain microglia in morphology, using GM-CSF and IL-34;  
33 the monocytes were incubated with GM-CSF and IL-34 for 14 d, which resulted

1 in a clear ramified shape, although the precise molecular mechanisms  
2 underlying this morphological change were not addressed. The morphology of  
3 ramified microglia obtained in the present study resembles *in vivo* microglia, and  
4 these microglia closely mimic the dynamics of process tips observed in the brain  
5 (Fig. 1 and Movie 1). Importantly, the induced ramified microglia exhibit a  
6 non-inflammatory phenotype (Fig. 7A–E), suggesting a greater correlation  
7 between microglial morphology and function.

8  
9 Recently, receptors for LysoPS have been deorphanized, proving that GPR34,  
10 P2Y10, and GPR174 are the LysoPS receptors (Makide et al. 2014). Among  
11 these receptors, GPR34 expression was shown in microglia (Hickman et al.  
12 2013; Liebscher et al. 2011), and we confirmed that GPR34 was predominantly  
13 expressed in primary cultured microglia (Fig. 2A). Previously, GPR-34-deficient  
14 mice resulted in slightly enlarged microglial somata and less branches per cell *in*  
15 *vivo* compared with WT mice (Preissler et al. 2015), although our cultured  
16 microglia did not show any significant difference in morphology between  
17 GPR34-deficient and WT cells (Fig. 2D). Notably, Gi and Gs inhibitors also failed  
18 to suppress ramification after LysoPS application. We tested other receptors for  
19 LysoPS, such as P2Y10 and GPR174, using their specific agonists (Ikubo et al.  
20 2015; Jung et al. 2016), and the results showed that these ligands had no effect  
21 on microglial morphology (Fig. 2B, C). Furthermore, the effective dose of  
22 LysoPS (approximately 10  $\mu$ M) was relatively greater, and dramatic increases in  
23 LysoPS and PS were observed inside the microglia after LysoPS treatment (Fig.  
24 4A). It is known that the *lyso*-forms of phospholipids are easily penetrated into  
25 cell membrane (Arouri and Mouritsen 2013), and this character of lysolipids is  
26 actually used to change localization of intracellular PS in yeast (Fairn 2011). As  
27 a general character of lysolipids, lysolipids are able to be incorporated into  
28 membrane and capable of changing lipid composition of membrane. Collectively,  
29 these data suggest that the changes observed in microglia following LysoPS  
30 treatment was not mediated *via* a receptor, but rather it is more likely that  
31 incorporation of LysoPS occurred *via* the plasma membrane and functioned  
32 within the microglia.

33

1 LysoPS is capable of being incorporated into the membrane (Arouri and  
2 Mouritsen 2013), subsequently flipping to the inner monolayer, and rapidly  
3 converting to PS *via* membrane-bound lysophospholipid acyltransferases: the  
4 deacylation / reacylation reaction is called the Lands cycle (Lands 1958;  
5 Shindou and Shimizu 2009). We confirmed increased LysoPS and PS levels in  
6 microglial cells using LC-MS/MS (Fig. 4A) and the GST-evt-2-PH probe, which  
7 specifically binds to PS head groups (Fig. 4C) (Uchida et al. 2011). Results  
8 showed significantly increased LysoPS and PS in microglia. The treatment of  
9 LysoPS with shorter or longer fatty acids did not sufficiently alter morphology  
10 (Fig. 3A, B), which could be due to differences in permeability depending on the  
11 length of acyl chains (Arouri and Mouritsen 2013; Hoyrup et al. 2001). To further  
12 address this, we used 1- and 2-deoxy-LysoPS that were not converted to PS by  
13 acyltransferases (Fig. 4B). Because these deoxy-LysoPS failed to induce  
14 ramification, it could be concluded that LysoPS incorporation and subsequent  
15 conversion to PS in microglia is crucial for altering microglial morphology.

16

17 Cell morphology is due to the reorganization of actin and microtubule  
18 cytoskeletons that are induced by a family of small RhoGTPases. We identified  
19 that the small RhoGTPase Cdc42 plays an essential role in LysoPS-induced  
20 ramification of microglia (Fig. 5A–E). Cdc42 exists in the plasma membrane and  
21 in endomembranes, such as the Golgi complex and endoplasmic reticulum  
22 (Farhan and Hsu 2016; Michaelson et al. 2001). In cultured microglia,  
23 endogenous Cdc42 was evenly localized in the eminent area of the plasma  
24 membrane, and abundantly in the endomembrane (Fig. 6A). Cdc42 associates  
25 with PS on the membrane when prenylated. Therefore, prenylation is necessary  
26 for Cdc42 to bind to membranes and become activated. When we inhibited  
27 Cdc42 prenylation with GGTI 298, a geranylgeranyltransferase inhibitor, Cdc42  
28 translocation to the cytoplasmic membrane, as well as ramification, was totally  
29 suppressed (Fig. 6A–E). Cdc42 possesses a carboxy-terminal cationic region in  
30 the vicinity of the isoprenylation site, which allows binding to phospholipids with  
31 a negative charge, such as PS. This may be why LPLs with a negative charge at  
32 polar head groups, such as LPI and LPG, were able to alter microglial  
33 morphology to some extent, whereas other non-negatively charged LPLs failed

1 (Fig. 3C, D). Although LPC does not have a negative charge, LPC slightly  
2 altered the morphology. Because PS is made by exchanging serine for the  
3 choline head groups of phosphatidylcholine (Vance and Tasseva 2013), LPC  
4 application might induce PS level. However, PS application did not alter  
5 morphology, which might be due to the lower penetration ability *via* the plasma  
6 membrane (Arouri and Mouritsen 2013). Although we do not know why the PS  
7 head groups are primarily accumulated in the primary and secondary shafts of  
8 microglia and not in further branched processes and tips (Fig. 6C), this restricted  
9 accumulation would be a crucial event for recruiting Cdc42 at the restricted  
10 process region. Conversely, the lack of PS and Cdc42 in the peripheral  
11 branches and tips might be important for maintaining motility. This local  
12 regulation of Cdc42 distribution on the plasma membrane could be a critical  
13 factor for microglia to change from an amoeboid to a ramified morphology.

14

15 As mentioned above, a higher correlation between microglial morphology and  
16 function is likely, even in cultured cells. Many results, including the present,  
17 indicate that a ramified microglial shape releases less pro-inflammatory  
18 cytokines, whereas an amoeboid shape secretes significant levels of  
19 pro-inflammatory cytokines (Saijo and Glass 2011). LysoPS has long been  
20 known as a signalling phospholipid in mast cell biology, markedly enhancing  
21 stimulated histamine release and eicosanoid production (Martin and Lagunoff  
22 1979), and was recently shown to be a mediator in activating clearance of dying  
23 cells by macrophages (Nishikawa et al. 2015). These actions are accompanied  
24 by pro-inflammatory responses rather than the anti-inflammatory functions  
25 mentioned in this paper (Fig. 7A–E). This difference could be due to the  
26 involvement of a receptor; the pro-inflammatory effects of LysoPS appear  
27 receptor-mediated, although the effect demonstrated in this study was receptor  
28 non-mediated. Although further evidence is needed to conclude that  
29 re-distributed Cdc42 exerts suppression of inflammatory responses, including  
30 the export of NF- $\kappa$ B from the nucleus, a change in Cdc42 intracellular  
31 localization could exert different functions (Farhan and Hsu 2016). Alternatively,  
32 the PS head groups, rather than Cdc42, may be involved in the suppression of  
33 inflammatory responses.

1 In conclusion, the present study addressed a mechanism underlying microglial  
2 ramification *in vitro*. The alteration of local phospholipid localization, which  
3 recruits the intracellular signalling molecule Cdc42, is pivotal. Composition of  
4 lipid species on the plasma membrane could be critical for characterizing cell  
5 morphology, as well as function, similar to the raft (Munro 2003); uneven  
6 localization of lipids on the plasma membrane locally recruits intracellular  
7 signalling molecules and induces local changes in plasma membrane  
8 morphology and function. The present study provides a tool to manipulate a  
9 microglial phenotype *in vitro*, and these results could promote further research  
10 on the microglial multifaceted functions exerted in response to surrounding  
11 environments.

12

1 **Acknowledgments**

2 We are grateful to T. Taguchi, T. Fujimoto, and T. Tsuji for technical advice and  
3 discussions, Ms. Y. Itai and Ms. M. Okamoto for technical assistance, and Ms. A.  
4 Asano for secretarial assistance. We also thank Ono Pharmaceutical Co., Ltd.  
5 for providing some forms of lysophospholipids. This work was supported by a  
6 Grant-in-Aid for JSPS Fellows (Grant Number 15J02662) and partly supported  
7 by a grant from the Ministry of Education, Culture, Sports, Science and  
8 Technology of the Japanese Government (numbers: 23111007, 16H05117,  
9 16K15170). K.T. is supported by research fellowships for Young Scientists from  
10 the Japan Society for the Promotion of Science.

11

1 ***Author contributions***

2 K.T. conducted most of the experiments and analyzed the data. H. Konishi  
3 performed SEM. K. M., H. Kawana. and J. A. provided the GPR34 KO mice, and  
4 performed LC-MS/MS. K. M., T. O. and J. A. provided agonist, and LysoPS  
5 analog. S. N. and K. K. provided AAV and performed western blot. K. T., H.  
6 Konishi and H. Kiyama designed the study and wrote the manuscript, with help  
7 from J. A. and K.K., and H. Kiyama conceived of and led the project.

8

1 **References**

- 2 Arouri A, Mouritsen OG. 2013. Membrane-perturbing effect of fatty acids and  
3 lysolipids. *Progress in Lipid Research* 52:130-140.
- 4 Bayer TA, Buslei R, Havas L, Falkai P. 1999. Evidence for activation of microglia  
5 in patients with psychiatric illnesses. *Neuroscience Letters* 271:126-128.
- 6 Boillee S, Yamanaka K, Lobsiger CS, Copeland NG, Jenkins NA, Kassiotis G,  
7 Kollias G, Cleveland DW. 2006. Onset and progression in inherited ALS  
8 determined by motor neurons and microglia. *Science* 312:1389-1392.
- 9 Bonizzi G, Karin M. 2004. The two NF-kappa B activation pathways and their  
10 role in innate and adaptive immunity. *Trends in Immunology* 25:280-288.
- 11 Butovsky O, Jedrychowski MP, Moore CS, Cialic R, Lanser AJ, Gabriely G,  
12 Koeglsperger T, Dake B, Wu PM, Doykan CE and others. 2014.  
13 Identification of a unique TGF-beta dependent molecular and functional  
14 signature in microglia. *Nature Neuroscience* 17:131-143.
- 15 Das A, Slaughter BD, Unruh JR, Bradford WD, Alexander R, Rubinstein B, Li R.  
16 2012. Flippase-mediated phospholipid asymmetry promotes fast Cdc42  
17 recycling in dynamic maintenance of cell polarity. *Nature Cell Biology*  
18 14:304-310.
- 19 Fairn GD, Hermansson M, Somerharju P, Grinstein S. 2011. Phosphatidylserine  
20 is polarized and required for proper Cdc42 localization and for  
21 development of cell polarity. *Nature Cell Biology* 13:1424-1430.
- 22 Farhan H, Hsu VW. 2016. Cdc42 and Cellular Polarity: Emerging Roles at the  
23 Golgi. *Trends in Cell Biology* 26:241-248.
- 24 Finkielstein CV, Overduin M, Capelluto DGS. 2006. Cell migration and signaling  
25 specificity is determined by the phosphatidylserine recognition motif of  
26 Rac1. *Journal of Biological Chemistry* 281:27317-27326.
- 27 Hanisch UK, Kettenmann H. 2007. Microglia: active sensor and versatile effector  
28 cells in the normal and pathologic brain. *Nature Neuroscience*  
29 10:1387-1394.
- 30 Henry EP, Peterson JR, Salvarezza SB, Rodriguez-Boulan E, Chen JL,  
31 Stamnes M, Macia E, Feng Y, Shair MD, Kirchhausen T. 2006.  
32 Secramine inhibits Cdc42-dependent functions in cells and Cdc42  
33 activation in vitro. *Nature Chemical Biology* 2:39-46.

1 Hickman SE, Kingery ND, Ohsumi TK, Borowsky ML, Wang LC, Means TK, El  
2 Khoury J. 2013. The microglial sensome revealed by direct RNA  
3 sequencing. *Nature Neuroscience* 16:1896-1905.

4 Hoyrup P, Davidsen J, Jorgensen K. 2001. Lipid membrane partitioning of  
5 lysolipids and fatty acids: Effects of membrane phase structure and  
6 detergent chain length. *Journal of Physical Chemistry B* 105:2649-2657.

7 Ikubo M, Inoue A, Nakamura S, Jung SJ, Sayama M, Otani Y, Uwamizu A,  
8 Suzuki K, Kishi T, Shuto A and others. 2015. Structure-Activity  
9 Relationships of Lysophosphatidylserine Analogs as Agonists of  
10 G-Protein-Coupled Receptors GPR34, P2Y10, and GPR174. *Journal of*  
11 *Medicinal Chemistry* 58:4204-4219.

12 Inoue A, Arima N, Ishiguro J, Prestwich GD, Arai H, Aoki J. 2011. LPA-producing  
13 enzyme PA-PLA(1) $\alpha$  regulates hair follicle development by  
14 modulating EGFR signalling. *Embo Journal* 30:4248-4260.

15 Inutsuka A, Inui A, Tabuchi S, Tsunematsu T, Lazarus M, Yamanaka A. 2014.  
16 Concurrent and robust regulation of feeding behaviors and metabolism by  
17 orexin neurons. *Neuropharmacology* 85:451-460.

18 Iwashita M, Makide K, Nonomura T, Misumi Y, Otani Y, Ishida M, Taguchi R,  
19 Tsujimoto M, Aoki J, Arai H and others. 2009. Synthesis and Evaluation of  
20 Lysophosphatidylserine Analogues as Inducers of Mast Cell  
21 Degranulation. Potent Activities of Lysophosphatidylthreonine and Its  
22 2-Deoxy Derivative. *Journal of Medicinal Chemistry* 52:5837-5863.

23 Jung S, Inoue A, Nakamura S, Kishi T, Uwamizu A, Sayama M, Ikubo M, Otani Y,  
24 Kano K, Makide K and others. 2016. Conformational Constraint of the  
25 Glycerol Moiety of Lysophosphatidylserine Affords Compounds with  
26 Receptor Subtype Selectivity. *Journal of Medicinal Chemistry*  
27 59:3750-3776.

28 Konishi H, Namikawa K, Kiyama H. 2006. Annexin III implicated in the microglial  
29 response to motor nerve injury. *Glia* 53:723-732.

30 Konishi H, Ogawa T, Nakagomi S, Inoue K, Tohyama M, Kiyama H. 2010. Id1,  
31 Id2 and Id3 are induced in rat melanotrophs of the pituitary gland by  
32 dopamine suppression under continuous stress. *Neuroscience*  
33 169:1527-1534.

- 1 Kreutzberg GW. 1996. Microglia: A sensor for pathological events in the CNS.  
2 Trends in Neurosciences 19:312-318.
- 3 Ladeby R, Wirenfeltd M, Garcia-Ovejero D, Fenger C, Dissing-Olesen L,  
4 Dahnau I, Finsen B. 2005. Microglial cell population dynamics in the  
5 injured adult central nervous system. Brain Research Reviews  
6 48:196-206.
- 7 Lands WEM. 1958. Metabolism of glycerolipides; a comparison of lecithin and  
8 triglyceride synthesis. Journal of Biological Chemistry 231:883-888.
- 9 Lazarus M, Shen HY, Cherasse Y, Qu WM, Huang ZL, Bass CE,  
10 Winsky-Sommerer R, Semba K, Fredholm BB, Boison D and others. 2011.  
11 Arousal Effect of Caffeine Depends on Adenosine A(2A) Receptors in the  
12 Shell of the Nucleus Accumbens. Journal of Neuroscience  
13 31:10067-10075.
- 14 Liebscher I, Muller U, Teupser D, Engemaier E, Engel KMY, Ritscher L, Thor D,  
15 Sangkuhl K, Ricken A, Wurm A and others. 2011. Altered Immune  
16 Response in Mice Deficient for the G Protein-coupled Receptor GPR34.  
17 Journal of Biological Chemistry 286:2101-2110.
- 18 Makide K, Uwamizu A, Shinjo Y, Ishiguro J, Okutani M, Inoue A, Aoki J. 2014.  
19 Novel lysophospholipid receptors: their structure and function. Journal of  
20 Lipid Research 55:1986-1995.
- 21 Martin TW, Lagunoff D. 1979. Interactions of lysophospholipids and mast cells.  
22 Nature 279:250-252.
- 23 May MJ, Ghosh S. 1998. Signal transduction through NF-kappa B. Immunology  
24 Today 19:80-88.
- 25 Michaelson D, Silletti J, Murphy G, D'Eustachio P, Rush M, Philips MR. 2001.  
26 Differential localization of Rho GTPases in live cells: Regulation by  
27 hypervariable regions and RhoGDI binding. Journal of Cell Biology  
28 152:111-126.
- 29 Morgan JT, Chana G, Pardo CA, Achim C, Semendeferi K, Buckwalter J,  
30 Courchesne E, Everall IP. 2010. Microglial Activation and Increased  
31 Microglial Density Observed in the Dorsolateral Prefrontal Cortex in  
32 Autism. Biological Psychiatry 68:368-376.
- 33 Muessel MJ, Harry GJ, Armstrong DL, Storey NM. 2013. SDF-1 and LPA

1 modulate microglia potassium channels through rho gtpases to regulate  
2 cell morphology. *Glia* 61:1620-1628.

3 Munro S. 2003. Lipid rafts: Elusive or illusive? *Cell* 115:377-388.

4 Neubrand VE, Pedreno M, Caro M, Forte-Lago I, Delgado M, Gonzalez-Rey E.  
5 2014. Mesenchymal Stem Cells Induce the Ramification of Microglia Via  
6 the Small RhoGTPases Cdc42 and Rac1. *Glia* 62:1932-1942.

7 Ni JJ, Wu Z, Peterets C, Yamamoto K, Qing H, Nakanishi H. 2015. The Critical  
8 Role of Proteolytic Relay through Cathepsins B and E in the Phenotypic  
9 Change of Microglia/Macrophage. *Journal of Neuroscience*  
10 35:12488-12501.

11 Nimmerjahn A, Kirchhoff F, Helmchen F. 2005. Resting microglial cells are  
12 highly dynamic surveillants of brain parenchyma in vivo. *Science*  
13 308:1314-1318.

14 Nishikawa M, Kurano M, Ikeda H, Aoki J, Yatomi Y. 2015.  
15 Lysophosphatidylserine has Bilateral Effects on Macrophages in the  
16 Pathogenesis of Atherosclerosis. *Journal of Atherosclerosis and*  
17 *Thrombosis* 22:518-526.

18 Ohgidani M, Kato TA, Setoyama D, Sagata N, Hashimoto R, Shigenobu K,  
19 Yoshida T, Hayakawa K, Shimokawa N, Miura D and others. 2014. Direct  
20 induction of ramified microglia-like cells from human monocytes: Dynamic  
21 microglial dysfunction in Nasu-Hakola disease. *Scientific Reports* 4:7.

22 Preissler J, Grosche A, Lede V, Le Duc D, Krugel K, Matyash V, Szulzewsky F,  
23 Kallendrusch S, Immig K, Kettenmann H and others. 2015. Altered  
24 Microglial Phagocytosis in GPR34-Deficient Mice. *Glia* 63:206-215.

25 Rosenstiel P, Lucius R, Deuschl G, Sievers J, Wilms H. 2001. From theory to  
26 therapy: Implications from an in vitro model of ramified microglia.  
27 *Microscopy Research and Technique* 54:18-25.

28 Saijo K, Glass CK. 2011. Microglial cell origin and phenotypes in health and  
29 disease. *Nature Reviews Immunology* 11:775-787.

30 Schildge S, Bohrer C, Beck K, Schachtrup C. 2013. Isolation and Culture of  
31 Mouse Cortical Astrocytes. *Jove-Journal of Visualized Experiments*:7.

32 Shindou H, Shimizu T. 2009. Acyl-CoA: Lysophospholipid Acyltransferases.  
33 *Journal of Biological Chemistry* 284:1-5.

- 1 Tokizane K, Konishi H, Yasui M, Ogawa T, Sasaki K, Minamino N, Kiyama H.  
2 2013. Continuous stress promotes expression of VGF in melanotroph via  
3 suppression of dopamine. *Molecular and Cellular Endocrinology*  
4 372:49-56.
- 5 Tsuda M, Shigemoto-Mogami Y, Koizumi S, Mizokoshi A, Kohsaka S, Salter MW,  
6 Inoue K. 2003. P2X(4) receptors induced in spinal microglia gate tactile  
7 allodynia after nerve injury. *Nature* 424:778-783.
- 8 Uchida Y, Hasegawa J, Chinnapen D, Inoue T, Okazaki S, Kato R, Wakatsuki S,  
9 Masaki R, Koike M, Uchiyama Y and others. 2011. Intracellular  
10 phosphatidylserine is essential for retrograde membrane traffic through  
11 endosomes. *Proceedings of the National Academy of Sciences of the*  
12 *United States of America* 108:15846-15851.
- 13 Uwamizu A, Inoue A, Suzuki K, Okudaira M, Shuto A, Shinjo Y, Ishiguro J,  
14 Makide K, Ikubo M, Nakamura S and others. 2015.  
15 Lysophosphatidylserine analogues differentially activate three LysoPS  
16 receptors. *Journal of Biochemistry* 157:151-160.
- 17 Vance JE, Tasseva G. 2013. Formation and function of phosphatidylserine and  
18 phosphatidylethanolamine in mammalian cells. *Biochimica Et Biophysica*  
19 *Acta-Molecular and Cell Biology of Lipids* 1831:543-554.
- 20 Wake H, Moorhouse AJ, Jinno S, Kohsaka S, Nabekura J. 2009. Resting  
21 Microglia Directly Monitor the Functional State of Synapses In Vivo and  
22 Determine the Fate of Ischemic Terminals. *Journal of Neuroscience*  
23 29:3974-3980.
- 24 Wilms H, Hartmann D, Sievers J. 1997. Ramification of microglia, monocytes  
25 and macrophages in vitro: Influences of various epithelial and  
26 mesenchymal cells and their conditioned media. *Cell and Tissue*  
27 *Research* 287:447-458.
- 28 Yeung T, Gilbert GE, Shi J, Silvius J, Kapus A, Grinstein S. 2008. Membrane  
29 phosphatidylserine regulates surface charge and protein localization.  
30 *Science* 319:210-213.
- 31  
32

## 1 Figure Legends

### 3 **FIGURE 1: Characterization of ramified microglia induced by LysoPS *in vitro*.**

5 (A, B) Images of primary cultured microglia after vehicle or 10  $\mu$ M of LysoPS  
6 treatment. Images were acquired by SEM. Scale bar, 10  $\mu$ m. (C, D) Images of  
7 primary cultured neurons and astrocytes after vehicle or 10  $\mu$ M of LysoPS  
8 treatment. After 1 h of incubation, cells were fixed and immunostained for beta III  
9 Tubulin (neuron) and GFAP (astrocyte). Scale bar, 40  $\mu$ m. (E) A time-lapse  
10 image of cultured microglia. Up to 10  $\mu$ M of LysoPS was added at time point 0'.  
11 The number in each panel indicates minutes before and after LysoPS treatment.  
12 Scale bar, 20  $\mu$ m. (F) Representative the number of microglial branch terminal  
13 points in each cell is measured at each time-point indicated after LysoPS  
14 treatment (n = 5 cells). (G) Representative microglial branch length ( $\mu$ m), from  
15 soma to the tip, is measured at each time-point after LysoPS treatment (n = 5  
16 branches). Note that after initial extension, tips exhibit repeated extension and  
17 retraction. (H) Representative overlay of individual microglial cell trajectories  
18 after either vehicle or LysoPS treatments for 2 h (n = 5 each). (I) The  
19 MetaMorph-based quantification of velocity of cell migration. Cells were tracked  
20 over a 2 h period. Data represent means  $\pm$  S.D. of 20 cells per group. <sup>###</sup>*P* < 0.01,  
21 Mann-Whitney Rank Sum test.

### 23 **FIGURE 2: Ramification of microglia induced by LysoPS is not** 24 **receptor-dependent.**

25 (A) Representative real-time RT-PCR SYBR green fluorescence history vs.  
26 cycle number of mRNA expression for GPR34 (red), P2Y10 (purple), GPR174  
27 (blue) and *glyceraldehydes-3-phosphate dehydrogenase* (GAPDH) (green) in  
28 microglial cDNA.  $\Delta R_n$  is the signal normalized to fluorescence intensity. (B)  
29 Primary cultured microglial cells are incubated with vehicle, 10  $\mu$ M of LysoPS, 5  
30  $\mu$ M of GPR34 agonist, 5  $\mu$ M of P2Y10 agonist, or 5  $\mu$ M of GPR174 agonist. After  
31 1 h of incubation, cells were fixed and immunostained for phalloidin. Scale bar,  
32 20  $\mu$ m. (C) Quantification of cell shape was performed by calculating the form  
33 factor =  $4\pi \times \text{area}/(\text{perimeter})^2$ . Data are mean  $\pm$  S.D. and 20 cells per condition.

1 Three independent experiments, at least, were quantified.  $###P < 0.001$ , a  
2 one-way ANOVA followed by the Dunnett's *post hoc* test. (D) GPR34-deficient  
3 (GPR34 KO) microglial cells are incubated with LysoPS. Data are mean  $\pm$  S.D.  
4 and 20 cells per condition. At least three independent experiments were  
5 quantified.  $###P < 0.001$ , Mann-Whitney Rank Sum test. Scale bar, 20  $\mu$ m.

6  
7 **FIGURE 3: Microglial responses to fatty acid chain length of LysoPS and**  
8 **other LPL members**

9 (A) Microglial cells were incubated with vehicle, 10:0-, 12:0-, 14:0-, 16:0-, 16:1-,  
10 18:0-, 18:1-, 20:4-, or 22:6-LysoPS, respectively, at concentration of 10  $\mu$ M each.

11 (B) Quantification of cell shape was calculated using the form factor. Data are  
12 mean  $\pm$  S.D.; 20 cells per condition were quantified in at least three independent  
13 experiments.  $##P < 0.01$ ,  $###P < 0.001$ , a one-way ANOVA followed by the

14 Dunnett's *post hoc* test. Scale bar, 20  $\mu$ m. (C) Primary cultured microglial cells  
15 were incubated with vehicle, PS, LysoPS, LPA, S1P, LPE, LPC, LPI, or LPG,  
16 respectively, at concentration of 10  $\mu$ M each, scale bar, 20  $\mu$ m. (D) The form  
17 factor was measured to quantify cell shape. Data are mean  $\pm$  S.D.. 20 cells per  
18 condition were measured in at least three independent experiments.  $###P <$   
19 0.001, a one-way ANOVA followed by the Dunnett's *post hoc* test.

20  
21 **FIGURE 4: LysoPS is rapidly incorporated into microglial cells and**  
22 **converted to PS.**

23 (A) Mass spectrometric determination of the area ratio of PS  
24 and LysoPS in microglial cells before and after (10 min and 1 h) LysoPS  
25 treatment. Data are mean  $\pm$  S.D.. Three independent experiments were  
26 performed.  $#P < 0.05$ ,  $###P < 0.001$ , a one-way ANOVA followed by the Dunnett's

27 *post hoc* test. (B) Primary cultured microglia were incubated with vehicle,  
28 18:1-LysoPS, 2-deoxy-LysoPS, or 1-deoxy-LysoPS, respectively, at 10  $\mu$ M, and  
29 stained with Alexa 594-labelled phalloidin. Scale bar = 20  $\mu$ m. (C) Microglial cells

30 were incubated with purified recombinant GST-evt-2-PH after fixation and  
31 labelled as described in the Materials and Methods. Either vehicle- or  
32 LysoPS-treated cells were stained with antibody against GST or Alexa  
33 594-labelled phalloidin. The most right column indicates merged images  
together with DAPI. Scale bar, 20  $\mu$ m.

1

2 **FIGURE 5: Cdc42 is involved in LysoPS-induced microglial ramification.**

3 (A) Representative images of microglia incubated with vehicle or 10  $\mu$ M of  
4 LysoPS for 60 min, in the presence of an inhibitor for each signalling pathway:  
5 10  $\mu$ M of KT5720, 20  $\mu$ M of LY294002, 10  $\mu$ M of Y27632, 20  $\mu$ M of U0126, 50  
6  $\mu$ M of NSC23766, or 10  $\mu$ M of ML141. (B, C) EGFP-tagged DN mutants of Rac1  
7 and Cdc42 were infected by AAV. Arrows indicate EGFP-positive microglial cells.  
8 The cell shapes were quantified by calculating the form factor. Data are mean  $\pm$   
9 S.D.. 20 cells were analyzed for each mutant in three independent experiments.  
10  $###P < 0.001$ , a one-way ANOVA followed by the Dunnett's *post hoc* test. (D, E)  
11 After 1 min of incubation, cell lysates were assayed for activation of the small  
12 RhoGTPase Rac1 and Cdc42, and normalized to total Rac1 and Cdc42 amount  
13 in cell lysates. Data are mean  $\pm$  S.E.M. of three independent experiments.  $^{\#}P <$   
14 0.05, Mann-Whitney Rank Sum test.

15

16 **FIGURE 6: Localization of Cdc42 and GST-evt-2 PH in microglia treated**  
17 **with LysoPS and suppression of ramification by geranylgeranylation**  
18 **inhibition.**

19 (A, B) Confocal images showing localization of GST-evt-2-PH (green), Cdc42  
20 (blue), and phalloidin (red) in microglia after LysoPS treatment. Bottom right of  
21 each image is the overlay image of GST-evt-2-PH, Cdc42, and phalloidin  
22 (merged). Note that GST-evt-2-PH and Cdc42 are intensely expressed in the  
23 soma and primary and secondary processes, but not in the further periphery.  
24 Scale bar, 20  $\mu$ m. (C) The boxed areas in B are shown at a higher magnification.  
25 Note the GST-evt-2-PH- and Cdc42-positive signals in similar regions of the  
26 primary process. Scale bar, 500 nm. (D, E) A geranylgeranylation inhibitor, GGTI  
27 298 (20  $\mu$ M: D, 50  $\mu$ M: E) suppresses LysoPS-induced ramification and alters  
28 localization of GST-evt-2-PH and Cdc42 in microglia after 60 min incubation with  
29 LysoPS and GGTI 298. Scale bar, 20  $\mu$ m.

30

31 **FIGURE 7: LysoPS suppresses the LPS-induced proinflammatory**  
32 **phenotype in primary microglia.**

33 Primary cultured microglia were obtained from WT (A) and GPR34-deficient (B)

1 mice (postnatal 1–2 days), and treated with bacterial LPS and either vehicle or  
2 LysoPS for 3 h. The mRNA for proinflammatory and anti-inflammatory markers  
3 were quantified by quantitative real-time RT-PCR. Results were normalized to  
4 and are shown as ratios to LPS-treated microglia cells. Values show mean  $\pm$  S.D.  
5 of three independent experiments.  $^{\#}P < 0.05$ ,  $^{\#\#}P < 0.01$ ,  $^{\#\#\#}P < 0.001$ , two-tailed  
6 unpaired Student's *t*-test. (C) Microglial cells were incubated with vehicle or 10  
7  $\mu$ M of LysoPS for 60 min in the presence or absence of LPS (100 ng/ml). The  
8 cells were simultaneously stained with p65 (green), DAPI (blue), and phalloidin  
9 (red). The column third from the left shows merged images, and the column  
10 fourth from the left shows the higher magnification in the merged images. (D)  
11 Line-scan graphs of representative cells to the right of each panel indicate  
12 fluorescent intensities of NF- $\kappa$ B p65 (green) and DAPI (blue) along the yellow  
13 lines. Scale bar, 20  $\mu$ m. (E) Localization of NF- $\kappa$ B p65 are represented by  
14 cytoplasm localization (yellow), cytoplasm and nuclear localization (grey), and  
15 nuclear localization (black). Data are means from 100 cells pooled from four  
16 individual experiments.

# Fig.1

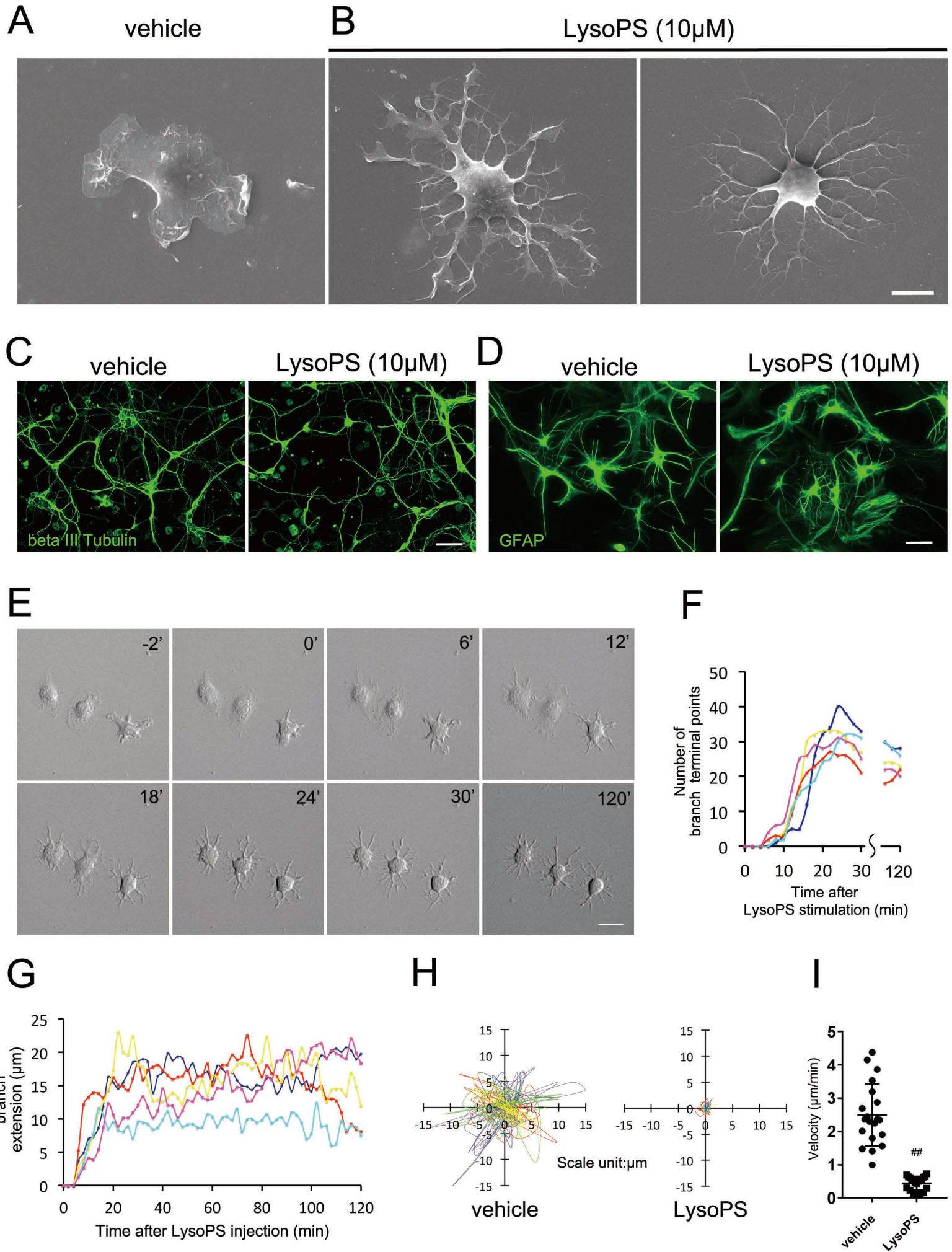


# Figure 2

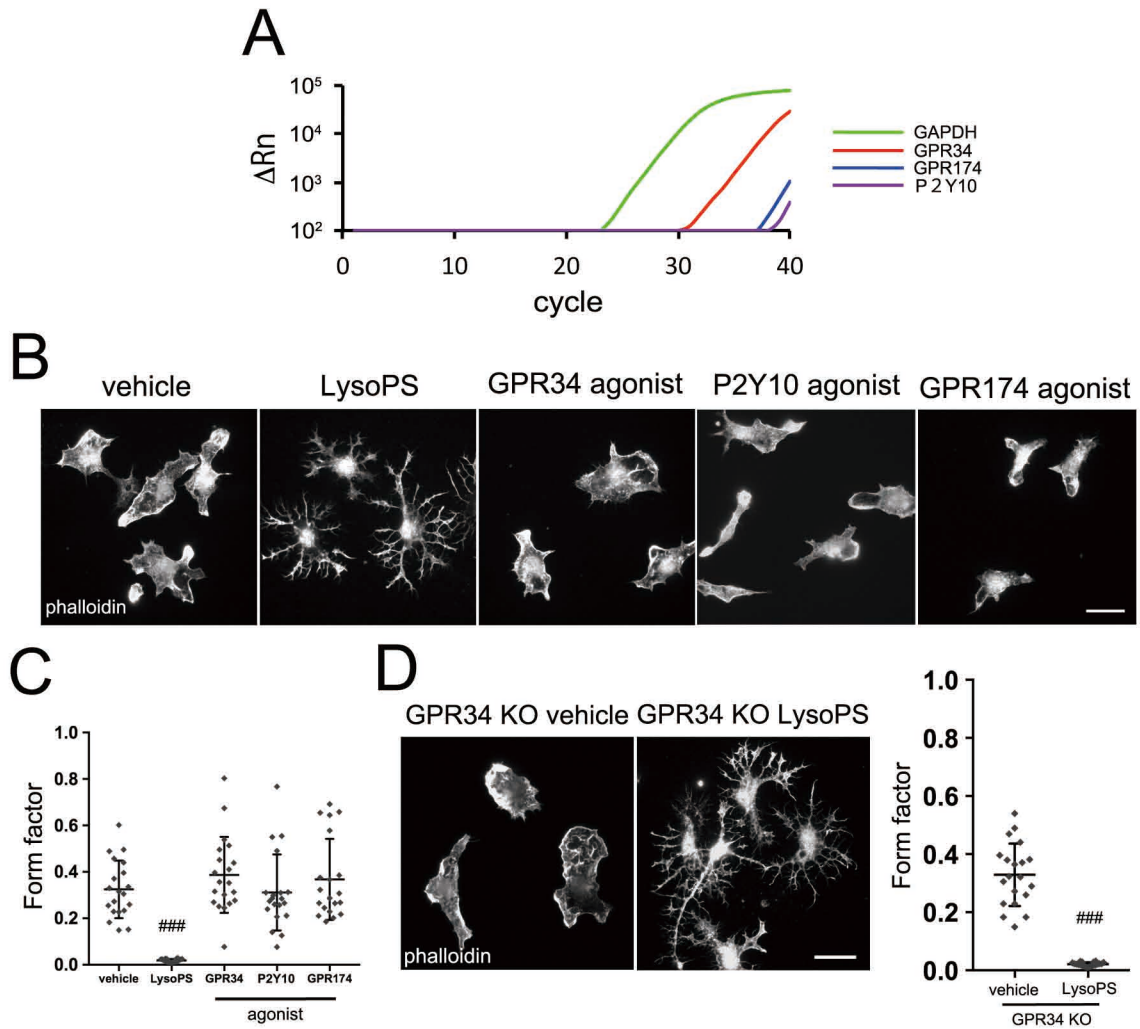


# Figure 3

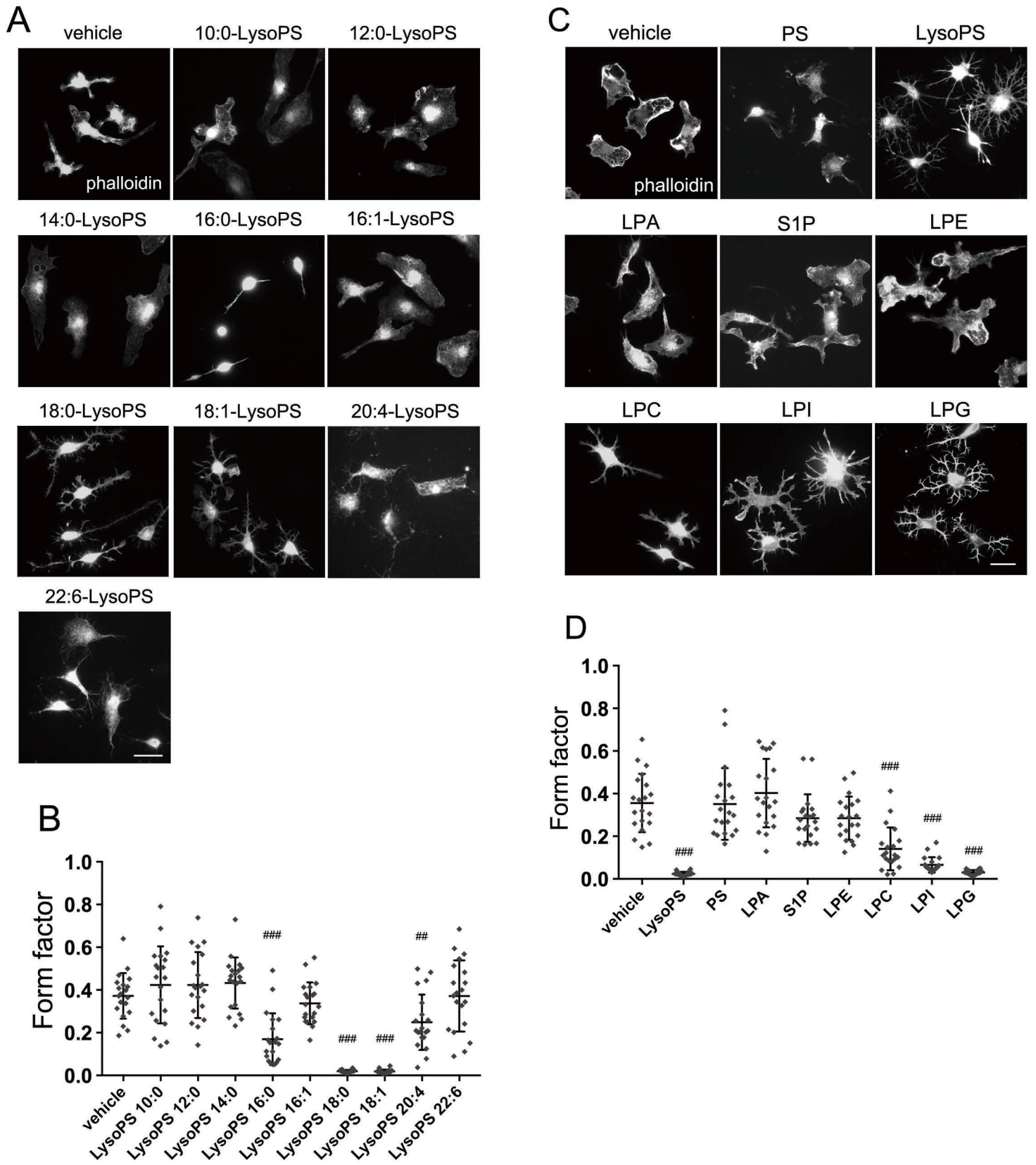
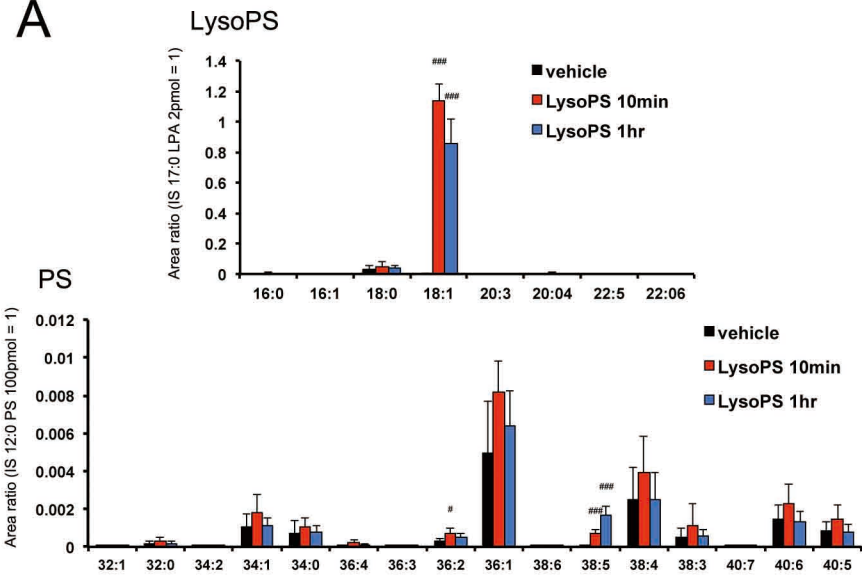
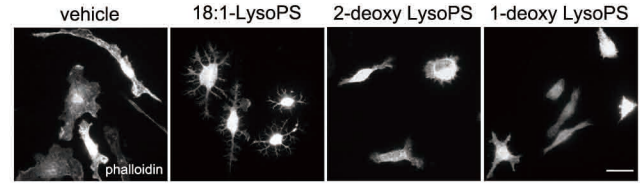


# Figure 4

**A**



**B**



**C**

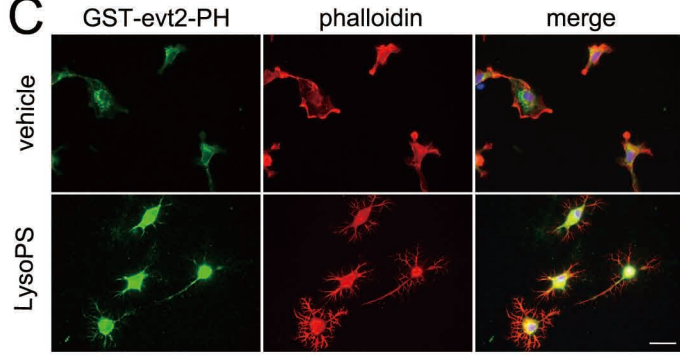


# Figure 5

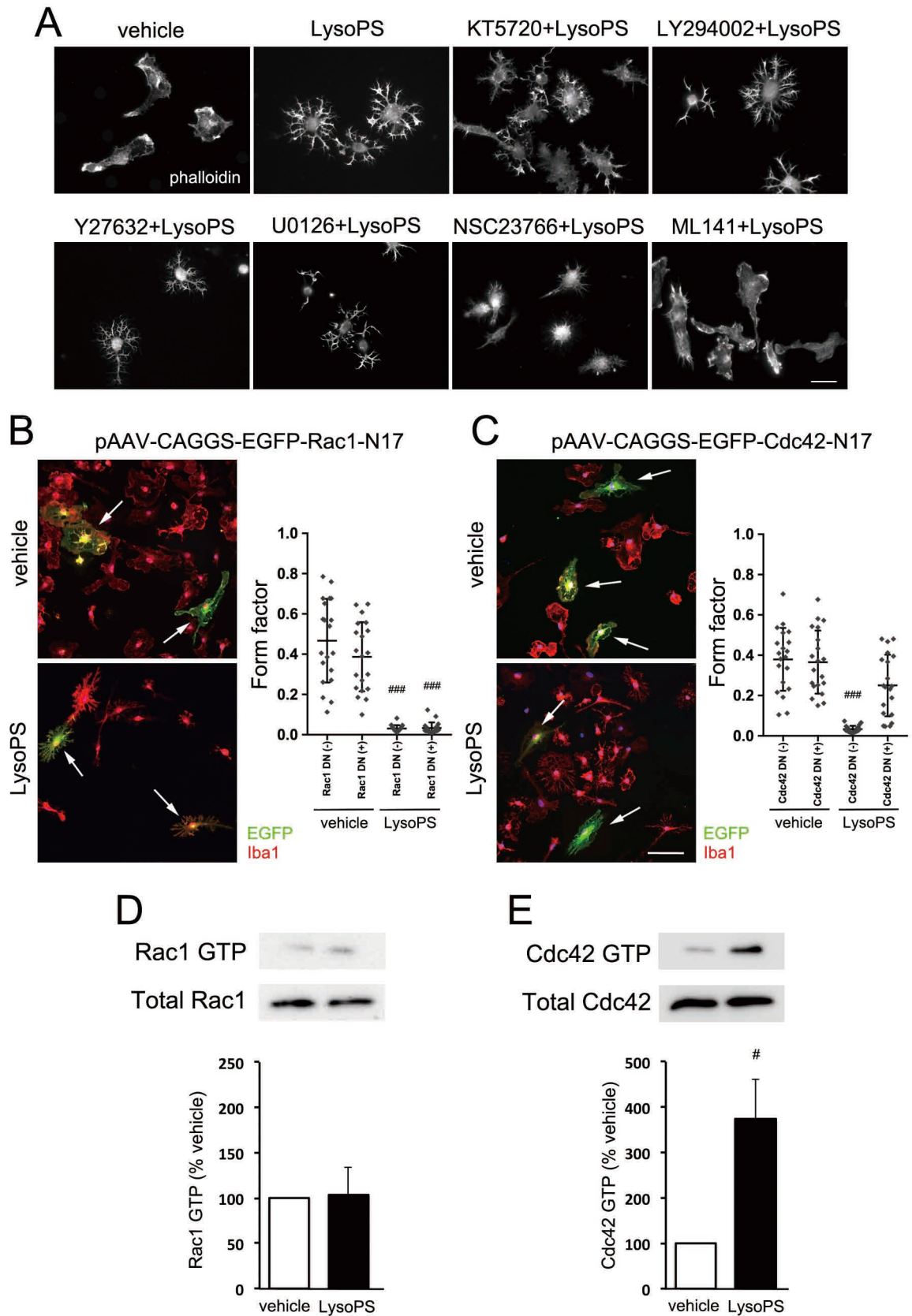


# Figure 6

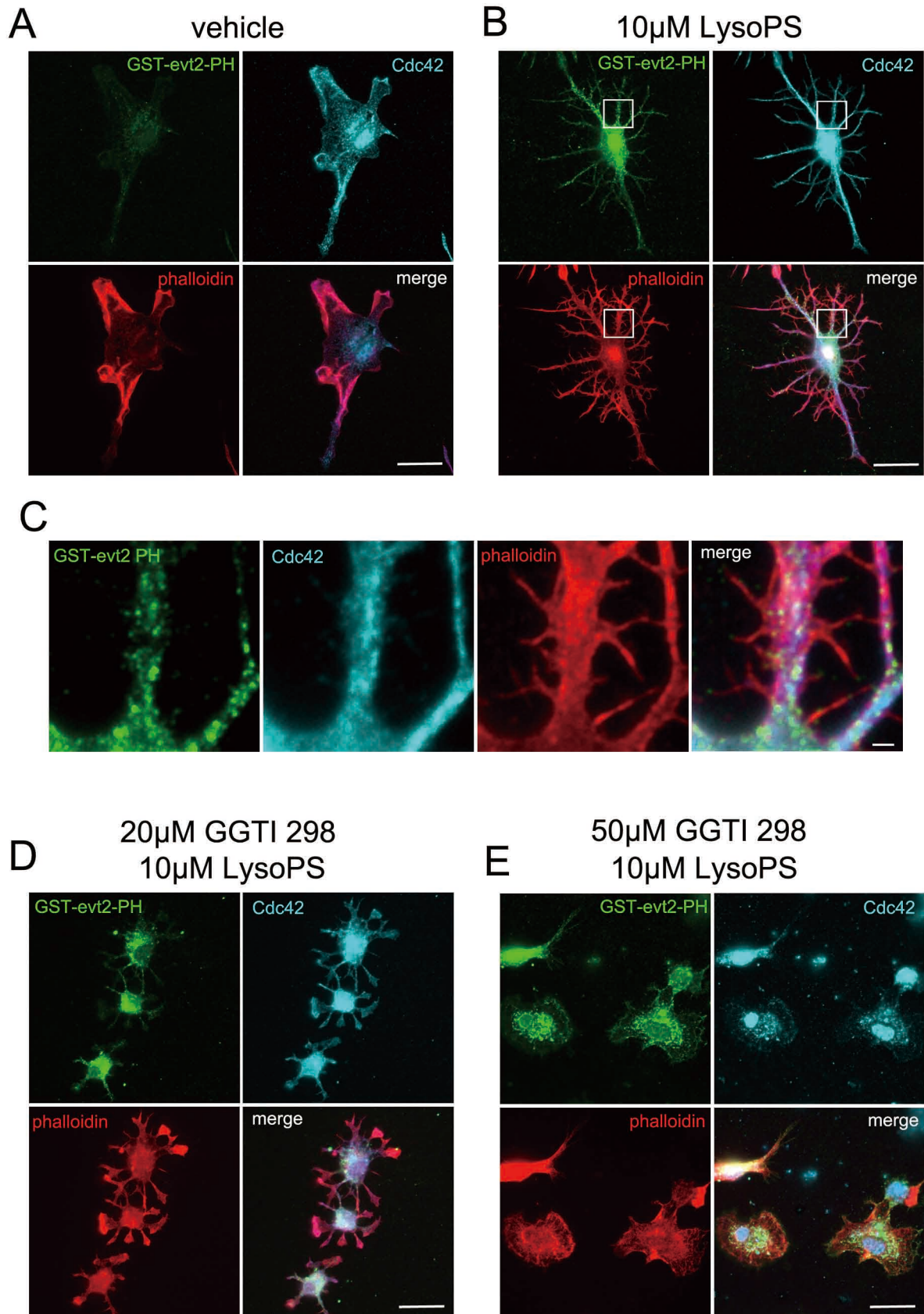


# Figure 7

